ACTION CAMS AND LOW-COST MULTI-FREQUENCY ANTENNAS FOR GNSS ASSISTED PHOTOGRAMMETRIC APPLICATIONS WITHOUT GROUND CONTROL POINTS

L. Morelli [a,b], F. Menna [a], A.Vitti [b], F. Remondino [a]

[a]3D Optical Metrology (3DOM) unit, Bruno Kessler Foundation (FBK), Trento, Italy
Web: http://3dom.fbk.eu – Email: <lmorelli><fmenna><remondino>@fbk.eu

[b]Dept. of Civil, Environmental and Mechanical Engineering (DICAM), University of Trento, Italy

Technical Commission II

KEY WORDS: Photogrammetry, GNSS, Direct Georeferencing, Ground Control Points, GoPro HERO9, ublox F9P, TOP106, 5k.

ABSTRACT:
In civil, architectural and environmental fields photogrammetry is one of the most common solutions for deriving geometric information about many kind of objects of interest. Photogrammetric surveys suffer for the need of ground control points (GCPs), well distributed over the survey area, to scale and georeference the produced 3D data. The placement of GCPs is both time-consuming and sometimes infeasible because of environmental constraints, such as vegetation on river sides. For aerial surveys with unmanned aerial vehicles (UAV), several studies have been proposed to use the UAV GNSS antenna to reduce or eliminate the need of GCPs. This technique, called GNSS-aided photogrammetry, has been little explored for terrestrial applications despite its potential in reducing surveying time, or for integrating terrestrial and aerial surveying. This gap has been partly caused by the high cost of topographic-grade GNSS, but in recent years the market has offered receivers, such as the ublox ZED-F9P, which can achieve high accuracy at low cost. In this work we propose a simple and fast GNSS-aided methodology for terrestrial photogrammetric surveys using low-cost GNSS and image sensors. The final aim is to create a general procedure to minimize survey costs and time, and derive a scaled and georeferenced 3D information without GCPs.

1. INTRODUCTION

3D models defined up to a scale in an arbitrary reference system can be automatically reconstructed from images using photogrammetry. Ground control points (GCPs) are necessary for scaling and georeferencing the model and to add constraints to the bundle block adjustment (Berra and Peppa, 2020). On the other hand, their placement and the related support survey, e.g., with a Global Navigation Satellite System (GNSS) device or a total station, can be difficult, dangerous, and time-consuming.
Photogrammetric surveys with unmanned aerial vehicles (UAV) have been widespread in the last few years, because of the final high-resolution outputs (orthophotos and DTMs), low-cost compared to aerial surveys, manageability, practicality in both rural and urban contexts, and finally the fast acquisition time (Jiang et al., 2021). But this last advantage is partially lost if GCPs have to be manually distributed and surveyed on the ground, stimulating researchers to avoid their use by taking advantage of the GNSS modules mounted onto UAVs. Real-time kinematic (RTK) and post-processed kinematic (PPK) technologies are mainly applied, reaching centimeter accuracies in the estimation of the centre of projection (COP) of the on-board camera, but limits the applications to the presence of a reference station near the survey area. There were some attempts to overcome this limitation using PPP (Grayson et al., 2018; Elsheikh et al., 2019), PPP-RTK or commercial solutions (ublox PointPerfect[1], POSPac PP-RTX[2]), to reach global operability.
The antenna phase centre (APC) coordinates are used to scale and georeference the 3D model, and as constraints in the bundle block adjustment (BBA). This approach is generally referred to as GNSS assisted photogrammetry, or sometimes improperly called direct georeferencing (Granshaw, 2020). The idea of aiding photogrammetry with GNSS or INS/GNSS is quite old (1984-early 2000s), but its diffusion was limited by the high cost of these devices (Forlani et al., 2014). With the spread of low-cost antennas and receivers, their application in the context of UAV surveys has become feasible. Most of the literature deals with almost planar survey areas (Zhang, 2019; Przybilla et al., 2020; Teppati Losè et al., 2020; Zeybek et al., 2021; Liu et al. 2022; Essel et al., 2022), while few works concentrate on surveying near-vertical objects, where the placement of GCPs is more difficult, impractical, or dangerous (Nesbit et al., 2022, Nocerino et al., 2012).

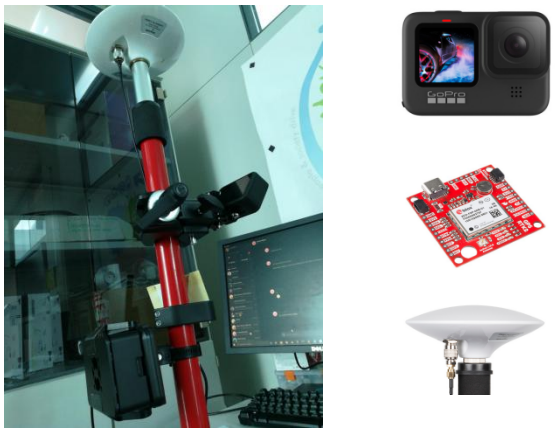

Figure 1: The proposed device (left); the GoPro HERO9 Balck, the SparkFun GPS-RTK2 with the ublox ZED-F9P module and the antenna TOP106 TOPGNSS (right).

Terrestrial photogrammetry is a valid alternative where UAV flights are not possible for environmental constraints or more often regulation restrictions. GCPs limit the operability of terrestrial photogrammetry as in the aerial case, but the topic is

[1] https://www.u-blox.com/en/product/pointperfect

[2] https://www.applanix.com/products/pospac8/pp-rtx.htm

little explored in literature. Jaud et al. (2020) leveraged a GNSS antenna rigidly coupled with an SLR camera for coastal reconstruction, while Forlani et al. (2014) mounted an SLR camera and a geodetic GNSS antenna on a pole for the 3D reconstruction of building facades, reaching accuracies of 3-7 cm in several tests. Similarly, a geotagging device using multi-constellation (GPS, GLONASS, Beidou, Galileo) and multichannel (L1, L2, L5) GNSS post processing PPK of Base-Rover configurations has been recently developed as a commercial product by REDcatch GmbH (www.redcatch.at).
In this paper, we couple an action cam and a low-cost GNSS antenna on a geodetic pole for terrestrial GNSS-aided photogrammetry without GCPs (Figure 1) and propose two operative survey pipelines: *static* and *kinematic*. We investigated both the use of geotagged photos and frames from 5k videos, which significantly decrease the acquisition time (Barazzetti et al., 2022). While Forlani et al. (2014) used pre-calibrated geodetic level devices, we explore a low-cost alternative, and we propose a general procedure for a rapid on-site calibration to calculate the lever-arm between the APC and the COP of the camera. The aim is to minimize the survey cost and time to obtain a scaled and georeferenced photogrammetric model without GCPs. In addition, the setup is very versatile, since sensors (e.g., multiple cameras, IMU, UWB) can be added and/or modified as needed and quickly calibrated in the field.

2. METHODOLOGY

2.1 Hardware

The bearing component of the device is a geodetic pole that hosts a TOPGNSS antenna TOP106[3] on the top end, and a GoPro HERO9 connected to the pole with a short arm. In this way, the camera and the antenna keep their mutual relative orientation constant during the survey. At the same time, the device can be used as a classic GNSS antenna to survey GCPs (if necessary), since the antenna is collinear to the pole screw. The antenna is connected to the SparkFun GPS-RTK2[4] board which mounts the ublox ZED-F9P[5] connected to a Raspberry Pi 4[6]. The Raspberry is accessible in SSH with the RaspController APP installed on a smartphone. Moreover, both the shutter of the GoPro and the GNSS receiver acquisition can be controlled using bash scripts.

2.2 Calibration

The paper evaluates two different procedures for terrestrial GNSS assisted photogrammetry that rely on a fast on-the-field calibration (Fig. 3-7b-7f), performed in RTK or in post-processing. For the *static* approach, the main steps of calibration follows (first chart of Fig. 2 and Fig. 3):
1. Survey of ~~at least~~ five, or more, GCPs with the GNSS antenna of the proposed device in static mode, placing the tip of the pole on each GCP. The number of GCPs was chosen to give some redundancy. Each target is surveyed for at least one minute, and post-processed separately as a static solution.
2. Acquisition of few photos with their GNSS position in static mode, following a circular path. It is not necessary to keep the pole vertical. In our test we acquired eight photos with their GNSS data, the red cameras in Fig. 3.
3. The geometry of the photogrammetric block is strengthened by adding other oblique images, without acquiring GNSS data to reduce the acquisition time (blue cameras in Fig. 3).
4. The images are used as input for a global or incremental reconstruction, to estimate position and camera orientations.
5. The GCPs can be automatically detected on the images and triangulated.
6. The 3D coordinates of the GCPs and the camera APC are used as constraints in a Bundle Block Adjustment (BBA) to estimate the lever-arm between the COP and the APC.

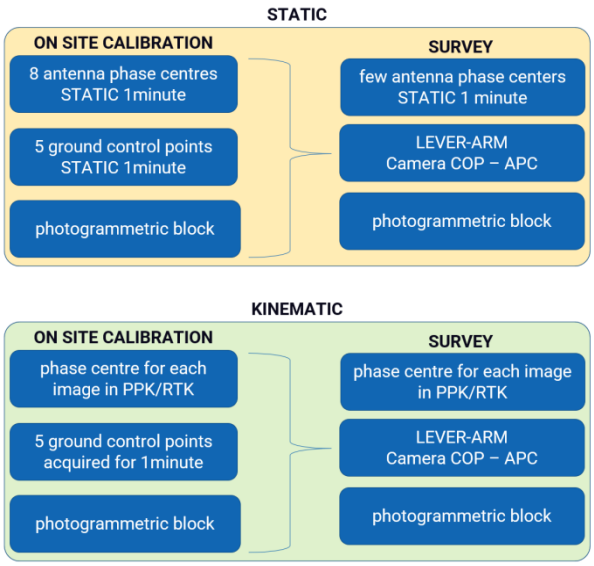

Figure 2: *Static* and *kinematic* survey approaches.

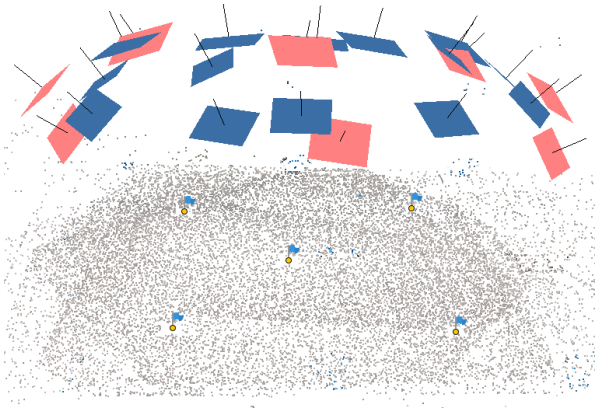

Figure 3: On-the-field calibration for the lever-arm estimation in the *static* approach.

The *kinematic* approach (second chart in Fig. 2) follows the same steps, however in this case the receiver starts acquiring the raw observation at the beginning of the calibration, then each target is surveyed for one minute, and finally the camera positions are acquired continuously while the device is moved in a loop-closure around the targets. The GNSS solution is calculated in post-processing or in real-time, assuming a moving device (kinematic mode).
In both approaches, the targets are acquired for one minute to help the solution to converge to a fix solution. In the future, we will also calculate the GNSS position in real-time to use the information of the type of solution (fix or float) as an indicator of

[3] https://cdn.sparkfun.com/assets/b/4/6/d/e/TOP106_GNSS_Antenna.pdf
[4] https://www.sparkfun.com/products/15136
[5] https://www.u-blox.com/en/product/zed-f9p-module
[6] https://www.raspberrypi.com/products/raspberry-pi-4-model-b/

the survey quality, so that when the solution is fix the operator can move to the next target.
This procedure is thought for a modular device, therefore the camera and the GNSS can be changed depending on the needs, and also be replaced with geodetic level devices. If the hardware is solidly coupled, the calibration can be re-executed only when needed.

2.3 Survey procedure

At survey time, the two approaches used in calibration can be applied (Figure 2). The *static* approach consists of acquiring a few well-distributed photos (e.g. 15 or 4) around the survey object and the GNSS data of their APCs, post-processed separately in static mode. Then, the photogrammetric block of images can be acquired, and, if necessary, the camera can be disconnected from the pole, free from the rest of the equipment. The BBA is constrained using the lever-arm calculated during the calibration, and the few GNSS positions acquired in static mode. Instead, the *kinematic* approach consists in continuously acquiring both GNSS observables and photos (time-lapse or video sequence). The images can be synchronised by leveraging the GPS timestamp from the GoPro internal receiver. The advantage is to have more data to constrain the BBA or have a better control of the GNSS and camera trajectories. Also in this case the lever-arm from the calibration is fixed in the BBA, and the GNSS position of each camera is used inside the BBA.
Note that the calibration is used only for the lever-arm calculation, while the interior parameters are re-estimated in self-calibration at survey time. Fixing the calibration interior parameters in the survey reconstruction, we obtained high deformations, suggesting that the calibration setup is too different from the actual survey to estimate reliable interior parameters. Instead, as will be shown in Sec. 3, the proposed calibration is enough reliable for the lever-arm estimation.

2.4 Elaboration of GNSS data

The opensource RTKLIB APIs (Takasu and Yasuda, 2009) were used for all the GNSS elaborations. Receiver observations were acquired in the field with the STR2STR API installed on the Raspberry Pi, and archived in *ubx* format. Offline, the raw observations were converted from *ubx* to RINEX with RTKCONV, and post-processed with RTKPOST. The solution was obtained by exploiting observables from a nearby permanent station, a few kilometres away. In all the performed tests, the computational approach was *post-processed kinematic* or *static*, using only the predicted orbits, to keep the analysis closer to real-time elaborations (RTK).

2.5 Site description

The test building is the East Building of the Fondazione Bruno Kessler (FBK), a reinforced concrete structure partially covered with metal panels (Figure 4). It has a one-story above ground floor for the South and East sides, and two stories above ground for the North and West sides. The acquisition path of both visual and GNSS sensors runs along a closed loop around the building perimeter and a few meters away from the facades (Figure 5). The survey device had complete visibility of the sky to the north, while on the east side there was another building of modest height that however left a good visibility of the sky. Instead, a bridge on North-West heavily affects the view of satellites below it and in its immediate vicinity. Finally, for half of the South and West facades, the visibility of satellites was partially obstructed by the presence of a tall retaining wall and some machinery.
The survey has its own challenges due to the presence of reflective surfaces that can generate multipath issues, and the partial obstruction of the sky in one of the sides of the building, similar to an urban canyon.

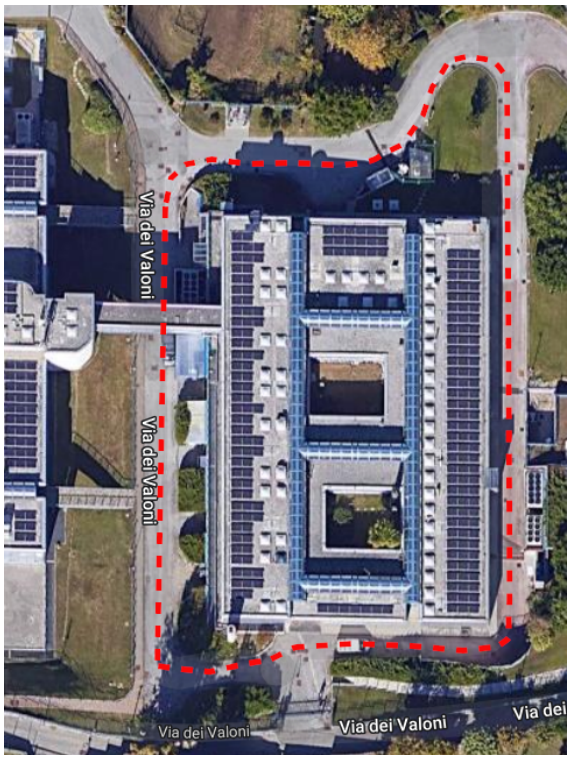

Figure 4: Orthophoto of the FBK building used for our tests. Image source: Google Maps.

3. RESULTS AND DISCUSSION

3.1 Static approach with few GNSS camera positions

To calculate the lever-arm offsets between the COP and the APC, we followed the procedure described in 2.2, displacing 5 ground control points on an outdoor ground plane and surveyed them with the ublox antenna integrated in the proposed device, as a classical GNSS survey. To keep the operations fast, each point was surveyed for 1 minute and post-elaborated in static mode. We checked the quality of these points, comparing them against a survey realized with a STONEX S8 Plus (with a longer static survey of 15 minutes). We obtained an error in planimetry and altimetry of 11±5 and 14±8 mm respectively. Then 22 images were acquired in a closed circular path with oblique images to strengthen the camera network geometry. To limit the acquisition time, for only eight images we acquired the position of the APC of the antenna for 1 minute in rapid static mode. See Figure 3 for the calibration setup.
We elaborated all the GNSS measurements in RTKLIB, while the lever-arm estimation was performed in Agisoft Metashape[7]. The residuals on the cameras met the expected figures, resulting in a root mean square error (RMSE) of 12 mm on the COPs, and 10 mm on the GCPs.
At survey time, we acquired 15 images with their GNSS data in rapid static mode for 1 minute, then the GoPro camera was disconnected from the device to acquire the photogrammetric

[7] https://www.agisoft.com/

block, shown in Figure 5, with a total of 603 images both normal and oblique to improve the self-calibration. Note that the previous calibration was used for the calculation of the lever-arm, but not for the camera calibration, since the calibration setup is not representative of the survey object. The photogrammetric block was oriented in Agisoft Metashape, fixing the lever-arm values found during the calibration, and using the 3D position of the 15 images to georeference and constrain the model during the BBA.

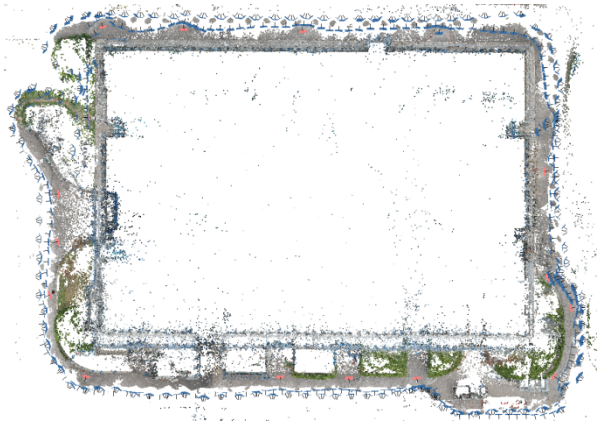

Figure 5: Plant view of the sparse reconstruction and camera network (blue frames) for the *static* approach with few GNSS camera positions. The images with GNSS data are in red.

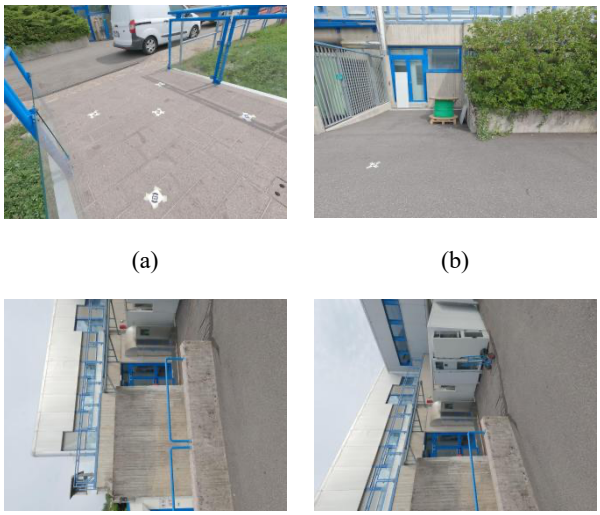

(a) (b)

(c) (d)

Figure 6: Examples of images acquired with the GoPro HERO 9. The calibration setup (a) and of the surveyed building (b-d).

To check the quality of the survey against a ground truth, on a different day 12 targets placed on the ground were surveyed with a STONEX S8 Plus to be used as check points (CPs). CP RMSEs, calculated between the estimated position of the targets in the photogrammetric model and the coordinates of the ground-truth, results in 12.7 mm and 26.5 mm in planimetry and altimetry respectively. If only 4 images are used to scale and georeference, the RMSE is slightly worse: 18.9 mm and 34.1 mm in planimetry and altimetry. In Table 1 the RMSE on both COPs and CPs are reported, while in Figure 6 some images of the calibration (a) and survey (b-d) are shown.

3.2 Kinematic approach with all GNSS camera position

In the second experiment, we tested the performance of the *kinematic approach* using the PPK solution associated with each image of the photogrammetric survey. Specifically, the GNSS receiver was started logging once at the beginning of the survey and remained in operation until the end. For both calibration and the actual survey, we stopped for a few seconds almost every meter to acquire the photo and the GNSS position.

The calibration phase, as in the previous test, involved surveying 5 points on the ground stopping for 1 minute on each, acquiring 16 photos in a circle (Fig. 7a, 7b). For each shot, the phase center of the GNSS antenna was calculated in PPK and entered into the Metashape BBA with the ground coordinates of the targets for the lever-arm calculation. To assign to each image its GNSS position, we synchronized the GPS time reported in the EXIF file of the images with the GPS time of the solution, comparing the tracks of the GNSS antenna and the camera reported in (Fig. 7a, 7b).

The photos used for calibration were not included in the reconstruction of the building. The survey consists of approximately one photo at one-meter intervals, with the camera axis orthogonal to the building. No oblique images were included, unlike the previous case for keeping the acquisition time limited. The results in terms of the RMSE on the CPs are 13.1 mm and 21.9 mm for the horizontal and vertical accuracy respectively, in line with the results of the previous test, which seems to indicate that a limited number of GNSS positions is sufficient to achieve good georeferencing and scaling of the model, when in presence of a robust camera network as the one of the first test. In any case, having a good redundancy of GNSS camera positions can alleviate problems related to accidentally disconnected photogrammetric blocks by independently georeferencing them.

3.3 Kinematic approach with frames from video

The third test investigates the potentials of an extremely fast survey, because GNSS raw data collection is started only once at the beginning of the survey, and image acquisition is done by a video obtained walking at almost constant speed around the building. The calibration is similar to the previous case, with the only difference that the camera never stops (see Fig 7e, 7f). Also in this test, as the previous one, the GNSS solution is PPK. The images were selected from the video to have one frame every second, and extracted to be synchronized with the 1Hz GNSS solution. 36 images with their GNSS position were used during calibration (Figure 7e, 7f), and the calculated lever-arm again was kept fixed at survey time. Also here, there is no inclusion of oblique images, while the entire acquisition lasted in total only eight minutes. The obtained vertical accuracy is 29.1 mm and is in line with the other tests. The horizontal accuracy is about 4 times worse, 57.7 mm, and probably due to the way the synchronization was performed. In fact, all the GNSS positions of the cameras are fix and not float, so the expected accuracy is like the other cases just above one centimetre.

In this case, the synchronization was more complex because the extracted frames didn't contain the GPS time-stamp or the internal clock information. So we synchronized manually the frames and the GNSS solution looking on the epoch of motion start, but an error of a few frames can have led to several cm of error horizontally, as visible in Table 1. In the future we will explore more accurate synchronization approaches that rely on the clock synchronization as in the first two tests.

TESTS	CALIBRATION				SURVEY			
	RMSE on ground control points [mm]		RMSE on COPs [mm]		RMSE on check points [mm]		RMSE on COPs [mm]	
	N-E Error	UP Error	N-E Error	UP Error	N-E Error	UP Error	N-E Error	UP Error
STATIC PHOTO 15 images with GNSS	4.7	8.5	3.9	11.2	12.7	26.5	7.2	12.6
STATIC PHOTO 4 images with GNSS	4.7	8.5	3.9	11.2	18.9	34.1	2.5	1.0
KINEMATIC RAPID-STATIC PHOTO ALL images with GNSS	5.2	5.0	2.7	5.2	13.1	21.9	9.5	13.6
KINEMATIC VIDEO NO OBLIQUE ALL images with GNSS	26.0	5.4	46.4	18.1	57.7	29.1	37.0	33.9

Table 1: RMSEs on the check points/ground control points and on the COPs, both at calibration and survey time.

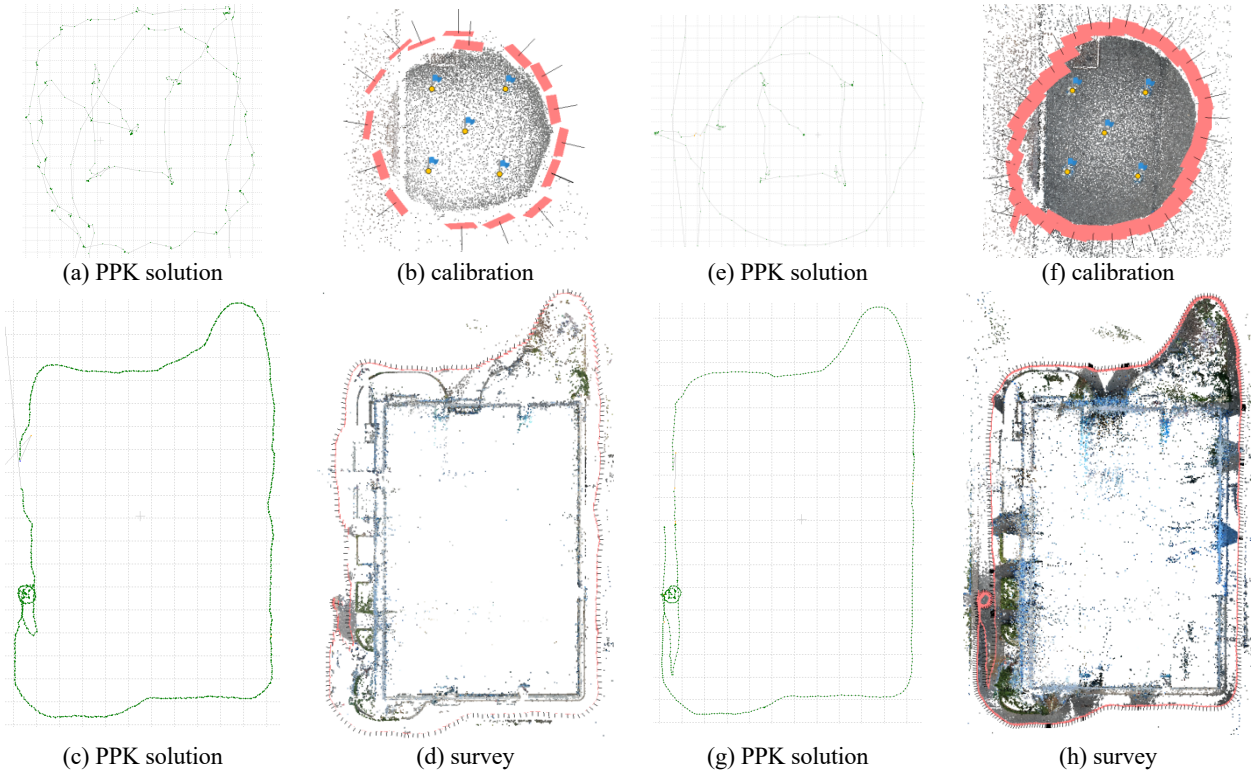

(a) PPK solution (b) calibration (e) PPK solution (f) calibration

(c) PPK solution (d) survey (g) PPK solution (h) survey

Figure 7: Calibration procedure (top row) and survey results (bottom row). Results for the rapid-static approach with all GNSS camera position (a-d) and same information for the kinematic approach with frames from video (e-h). In (b, d, f, h) the Metashape sparse clouds and camera positions are shown with red frames, the PPK solutions processed with RTKLIB are shown in (a, e, c, d).

4. CONCLUSIONS AND FUTURE WORK

The use of ground control points is still the state of the art for scaling and georeferencing a photogrammetric model. To overcome these limitations, the coordinates provided by a GNSS antenna solidly coupled to the camera can be used, if the lever-arm is known. In this paper, we proposed to couple a low-cost camera and GNSS antenna to georeference the photogrammetric models without ground-control points. We also proposed two operating procedures to minimize the survey time. The lever-arm can be calculated with an on the field calibration by placing 5 targets on the ground and acquiring a limited number of photographs in a loop-closure. At surveying time, only a few images need to be acquired along with their GNSS position to scale and georeference the model. If the camera network is sufficiently robust, using GNSS coordinates for all images does not lead to a significant improvement in accuracy. In any case, GNSS data redundancy can be useful in joining accidentally separated photogrammetric blocks. In future work, we will extend the analysis with other case studies, also testing the aid of other sensors such as inertial navigation systems and

ultrawideband devices. Replacing the action cam with a 360° spherical camera will be also considered, as in Barazzetti et al. (2022), which points out the difficulty in finding reliable matches between frames affected by significant illumination changes. To overcome these limitations, new local features based on neural networks could be tested, since they are trained to be robust under strong variations in the view angle and radiometric content (Remondino et al., 2021; Bellavia et al., 2022).

REFERENCES

Barazzetti, L., Previtali, M. and Roncoroni, F., 2022. 3D modelling with 5K 360° videos. In *9th International Workshop on 3D Virtual Reconstruction and Visualization of Complex Architectures, 3D-ARCH 2022* (Vol. 46, No. 2, pp. 65-71). International Society for Photogrammetry and Remote Sensing.

Bellavia, F., Morelli, L., Menna, F. and Remondino, F., 2022. Image Orientation with a Hybrid Pipeline Robust to Rotations and Wide-Baselines. *The International Archives of Photogrammetry, Remote Sensing and Spatial Information Sciences*, *46*, pp.73-80.

Berra, E.F. and Peppa, M.V., 2020, March. Advances and Challenges of UAV SFM MVS Photogrammetry and Remote Sensing: Short Review. In *2020 IEEE Latin American GRSS & ISPRS Remote Sensing Conference (LAGIRS)* (pp. 533-538). IEEE.

Elsheikh, M., Abdelfatah, W., Noureldin, A., Iqbal, U. and Korenberg, M., 2019. Low-cost real-time PPP/INS integration for automated land vehicles. *Sensors*, *19*(22), p.4896.

Essel, B., McDonald, J., Bolger, M. and Cahalane, C., 2022. Initial study assessing the suitability of drones with low-cost GNSS and IMU for mapping over featureless terrain using direct georeferencing. *The International Archives of Photogrammetry, Remote Sensing and Spatial Information Sciences*, *43*, pp. 37-44.

Forlani, G., Pinto, L., Roncella, R. and Pagliari, D., 2014. Terrestrial photogrammetry without ground control points. *Earth Science Informatics*, *7*(2), pp.71-81.

Granshaw, S.I., 2020. Photogrammetric terminology. *The Photogrammetric Record*, *35*(170), pp.143-288.

Grayson, B., Penna, N.T., Mills, J.P. and Grant, D.S., 2018. GPS precise point positioning for UAV photogrammetry. *The photogrammetric record*, *33*(164), pp.427-447.

Janos, D., Kuras, P. and Ortyl, Ł., 2022. Evaluation of low-cost RTK GNSS receiver in motion under demanding conditions. *Measurement*, *201*, p.111647.

Jaud, M., Bertin, S., Beauverger, M., Augereau, E. and Delacourt, C., 2020. RTK GNSS-assisted terrestrial SfM photogrammetry without GCP: Application to coastal morphodynamics monitoring. *Remote Sensing*, *12*(11), p.1889.

Jiang, S., Jiang, W. and Wang, L., 2021. Unmanned Aerial Vehicle-Based Photogrammetric 3D Mapping: A Survey of Techniques, Applications, and Challenges. *IEEE Geoscience and Remote Sensing Magazine*.

Liu, X., Lian, X., Yang, W., Wang, F., Han, Y. and Zhang, Y., 2022. Accuracy assessment of a UAV direct georeferencing method and impact of the configuration of ground control points. *Drones*, *6*(2), p.30.

Nesbit, P.R., Hubbard, S.M. and Hugenholtz, C.H., 2022. Direct georeferencing UAV-SfM in high-relief topography: Accuracy assessment and alternative ground control strategies along steep inaccessible rock slopes. *Remote Sensing*, *14*(3), p.490.

Nocerino, E., Menna, F. and Remondino, F., 2012, September. GNSS/INS aided precise re-photographing. In *2012 18th International Conference on Virtual Systems and Multimedia* (pp. 235-242). IEEE.

Remondino, F., Menna, F. and Morelli, L., 2021. Evaluating hand-crafted and learning-based features for photogrammetric applications. *The International Archives of Photogrammetry, Remote Sensing and Spatial Information Sciences*, *43*, pp.549-556.

Semler, Q., Mangin, L., Moussaoui, A. and Semin, E., 2019. Development of a low-cost centimetric GNSS positioning solution for Android applications. *International Archives of the Photogrammetry, Remote Sensing & Spatial Information Sciences*, 42-2-W17.

Takasu, T. and Yasuda, A., 2009, November. Development of the low-cost RTK-GPS receiver with an open source program package RTKLIB. In *International symposium on GPS/GNSS* (Vol. 1). International Convention Center Jeju Korea.

Teppati Losè, L., Chiabrando, F. and Giulio Tonolo, F., 2020. Boosting the timeliness of UAV large scale mapping. Direct georeferencing approaches: Operational strategies and best practices. *ISPRS International Journal of Geo-Information*, *9*(10), p.578.

Przybilla, H.J., Bäumker, M., Luhmann, T., Hastedt, H. and Eilers, M., 2020. Interaction between direct georeferencing, control point configuration and camera self-calibration for RTK-based UAV photogrammetry. *International Archives of the Photogrammetry, Remote Sensing & Spatial Information Sciences*, 43-B1-2020, 485-492.

Zahradník, D., Vyskočil, Z. and Hodík, Š., 2022. UBLOX F9P for geodetic measurement. *Stavební obzor-Civil Engineering Journal*, *31*(1), pp.110-119.

Zeybek, M., 2021. Accuracy assessment of direct georeferencing UAV images with onboard global navigation satellite system and comparison of CORS/RTK surveying methods. *Measurement Science and Technology*, *32*(6), p.065402.

Zhang, H., Aldana-Jague, E., Clapuyt, F., Wilken, F., Vanacker, V. and Van Oost, K., 2019. Evaluating the potential of PPK direct georeferencing for UAV-SfM photogrammetry and precise topographic mapping. *Earth Surf. Dyn. Discuss*, *7*, pp.807-827.